Russian Geology and Geophysics
Vol. 47, No. 5, pp. 557-567, 2006

Geologiya i Geofizika
UDC 550.834

PARTICLE MOTION OF PLANE WAVES IN VISCOELASTIC ANISOTROPIC MEDIA

V. Červený and I. Pšenčík*

Department of Geophysics, Faculty of Mathematics and Physics, Charles University, 3 Ke Karlovu, 121 16 Praha 2, Czech Republic
** Geophysical Institute, Academy of Sciences of Czech Republic, Boční II, 141 31 Praha 4, Czech Republic*

Particle motion of homogeneous and inhomogeneous time-harmonic plane waves propagating in unbounded viscoelastic anisotropic media is generally elliptical. Exception is linear polarization of *P* and *S* waves propagating along some specific directions. A typical example is a linear polarization of *SH* waves propagating in a plane of symmetry of a viscoelastic anisotropic medium. Two most important characteristics of the particle motion are the orientation of the axes of the polarization ellipse and its eccentricity. They both usually vary considerably with the direction of wavefront propagation, and with varying strength of inhomogeneity of the considered plane wave. The orientation of the *P*-wave polarization ellipse generally differs from the direction of wavefront propagation, and it is usually closer to the direction of the energy flux. The orientation of the polarization ellipses of *S* waves often differs from the direction perpendicular to the wavefront propagation, and it is usually closer to the direction perpendicular to the direction of the energy flux. The eccentricity of the polarization ellipse depends particularly strongly on the inhomogeneity of the plane wave. For homogeneous plane waves, the particle motion is usually nearly linear, i.e., polarization ellipses have large eccentricity, and the eccentricity decreases with increasing inhomogeneity of the wave. For strongly inhomogeneous plane waves, the polarization ellipse becomes nearly circular, eccentricity being very small. The eccentricity of the polarization ellipse usually also decreases in the vicinity of singular directions.

Viscoelastic anisotropic medium, polarization, homogeneous and inhomogeneous plane waves

INTRODUCTION

We investigate the particle motion of homogeneous and inhomogeneous time-harmonic plane waves propagating in an unbounded viscoelastic anisotropic medium in an arbitrarily specified direction. The plane wave is specified by the relation

$$u_j(x_k, t) = U_j \exp[-i\omega(t - p_n x_n)], \tag{1}$$

where x_k are Cartesian coordinates, u_j, p_j, and U_j are Cartesian components of the complex-valued displacement vector **u**, slowness vector **p** and amplitude vector **U**, respectively. Moreover, t is time and ω is a fixed, positive real-valued circular frequency. Equation (1) represents a plane wave if, and only if, U_j and p_j are chosen in such a way that (1) satisfies the equation of motion. This requirement yields a system of three linear equations for U_1, U_2, and U_3:

$$a_{ijkl}\, p_j\, p_l\, U_k = U_i, \quad i = 1, 2, 3. \tag{2}$$

Here a_{ijkl} are complex-valued, frequency-dependent, density-normalized viscoelastic moduli. We assume that they satisfy the symmetry relations $a_{ijkl} = a_{jikl} = a_{ijlk} = a_{klij}$. The corresponding 6×6 matrix $\boldsymbol{A}$ of density-normalized

viscoelastic moduli in the Voigt notation has $\mathrm{Re}\,\boldsymbol{A}$ positive definite and $-\mathrm{Im}\,\boldsymbol{A}$ positive definite or zero. The condition of solvability of the system of equations (2) reads

$$\det\left[a_{ijkl}\,p_j\,p_l - \delta_{ik}\right] = 0. \tag{3}$$

Constraint relation (3) can be used to determine the slowness vector **p**. When the relevant complex-valued slowness vector **p** is determined, it can be used in Equation (2) to calculate the amplitude vector **U**, from which the particle motion can be determined.

1. DETERMINATION OF THE SLOWNESS VECTOR p AND THE AMPLITUDE VECTOR U

The basic obstacle in studying particle motion of the plane wave (1) in viscoelastic anisotropic media is not the solution of Eq. (2) for **U**, but the determination of the slowness vector **p**, which satisfies (3). Commonly, the slowness vector is specified in the form $p_i = P_i + iA_i$, where P_i is the real-valued propagation vector (perpendicular to the wavefront), oriented in the direction of the propagation of the wavefront, and A_i is the real-valued attenuation vector (perpendicular to the plane of constant amplitude), oriented in the direction of the maximum decay of amplitudes. If A_i is parallel to P_i, the plane wave is called homogeneous, and if A_i and P_i make a nonzero angle, called the attenuation angle, the plane wave is called inhomogeneous. By introducing real-valued unit vectors $\mathbf{N} = \mathbf{P}/|\mathbf{P}|$ and $\mathbf{M} = \mathbf{A}/|\mathbf{A}|$, we can seek the slowness vector **p** in the form:

$$p_i = C^{-1}(N_i + i\delta M_i), \tag{4}$$

where N_i and M_i are assumed to be known, C is the real-valued phase velocity, and the quantity δ is an additional real-valued constant. The phase velocity C and δ are sought parameters. They can be determined from the equation obtained by inserting (4) into (3). Specification (4) is a generalization of the specification $p_i = C^{-1}N_i$, used broadly in perfectly elastic anisotropic media, which leads to the conventional eigenvalue problem for a 3×3 real-valued Christoffel matrix $\Gamma_{ik} = a_{ijkl}N_jN_l$. See, for example, [1–6]. Specification (4) has been broadly used to study inhomogeneous plane waves propagating in viscoelastic isotropic media, see for example, [1, 7–11]. Equation (4) can also be used for homogeneous plane waves ($N_i = M_i$) propagating in viscoelastic anisotropic media. Then $p_i = C^{-1}(1 + i\delta)N_i$. For inhomogeneous plane waves propagating in viscoelastic anisotropic media, however, Eqs. (3) and (4) yield a system of two coupled polynomial equations for C^2 and δ, which are of the third degree in C^2 and of the sixth degree in δ. Simpler systems of equations are obtained only for simpler cases like *SH* waves propagating in a plane of symmetry [9, 12–15]. An additional disadvantage of the system of equations based on the specification (4) is that for viscoelastic anisotropic media it yields $C^2 < 0$ for certain combinations of **N** and **M**. For discussion of this physically unacceptable result see [13, 14].

More convenient specification of the slowness vector, useful both in perfectly elastic and viscoelastic anisotropic media, reads:

$$p_i = \sigma n_i + p_i^{\Sigma} \text{ with } p_i^{\Sigma}\cdot n_k = 0. \tag{5}$$

Here **n** is a real-valued unit vector and $\mathbf{p}^{\Sigma}$ is a complex-valued vector, perpendicular to **n**. For **n** and $\mathbf{p}^{\Sigma}$ given, the scalar complex-valued quantity σ can be determined by solving an equation resulting from insertion of (5) into (3). The equation for σ is an algebraic equation of the sixth degree, with complex-valued coefficients. Alternatively, σ can be determined as an eigenvalue of a 6×6 complex-valued matrix. Specification (5) has been broadly used to calculate slowness vectors of waves generated by reflection/transmission at a plane interface separating perfectly elastic anisotropic media [4, 16, 17], and in the computation of displacement-stress (or velocity-stress) propagator matrices in 1-D isotropic and anisotropic structures [18–23]. In some of the mentioned references, viscoelastic media are also considered. An approach similar to the latter one, usually called Stroh formalism, was proposed by Stroh [24]. Stroh formalism has been applied to plane waves propagating in perfectly elastic, viscoelastic and thermoviscoelastic anisotropic media [25–27] and to the problems of reflection/transmission of plane waves at a plane interface separating viscoelastic anisotropic media [28].

Most suitable specification of the slowness vector for study of homogeneous and inhomogeneous plane waves propagating in a given direction **n** (perpendicular to the wavefront) in unbounded viscoelastic anisotropic media is the so-called mixed specification [29–31]:

$$p_i = \sigma n_i + iDm_i \text{ with } n_k\cdot m_k = 0. \tag{6}$$

Equation (6) is a special case of (5), with $\mathbf{p}^{\Sigma}$ purely imaginary. In (6), **n** and **m** are real-valued, mutually perpendicular unit vectors. It is obvious that the vector **n** is parallel to the propagation vector **P** so that **n** is also perpendicular to the wavefront. The two vectors, **n** and **m** specify the so-called propagation-attenuation plane $\Sigma^{\|}$. The vectors **P** and **A** are situated in it. The scalar real-valued parameter D ($-\infty < D < \infty$), is a so-called inhomogeneity parameter; $|D|$ is a measure of the inhomogeneity of a plane wave. The plane wave is homogeneous if $D = 0$ and inhomogeneous if $D \neq 0$. The vectors **n** and **m**, and the inhomogeneity parameter D represent the parameters of the plane wave under consideration, and may be chosen arbitrarily.

The complex-valued scalar quantity σ in (6) is a quantity to be determined. Algebraic equation for σ can be obtained by inserting (6) into (3):

$$\det [a_{ijkl} (\sigma n_j + iDm_j) (\sigma n_l + iDm_l) - \delta_{ik}] = 0. \tag{7}$$

Equation (7) is of the sixth degree with complex-valued coefficients. Its six roots correspond to three plane-wave modes, P, S_1 and S_2, propagating along and against **n**. In special cases, particularly in planes of symmetry, Eq. (7) can be factorized to equations of the fourth and second degree, and their solutions can be sought analytically.

Once Eq. (7) is solved for σ, the relevant slowness vector can be determined from (6), and the system (2) can be solved for **U**. The amplitude vector inserted into (1) yields complex-valued displacement vector **u**. In the following numerical examples we study particle motion of plane waves propagating in viscoelastic anisotropic media. Particle motion is defined as the locus of the end points of the real-valued displacement vector $\mathrm{Re}\mathbf{u}(x_k, t)$ at x_k for t varying. From (1) we get

$$\mathrm{Re}u_j (x_k, t) = (\mathrm{Re}U_j) \cos [\omega(t - p_m x_m)] - (\mathrm{Im}U_j) \sin [\omega(t - p_m x_m)]. \tag{8}$$

2. NUMERICAL EXAMPLES. PARTICLE MOTION DIAGRAMS

Here we investigate numerically the polarization of homogeneous and inhomogeneous plane P, S_1 and S_2 waves propagating in an unbounded viscoelastic anisotropic medium. Five different models are used: a) Model MJ of Jakobsen et al. [32] of a viscoelastic medium of hexagonal symmetry; b) Model MJ ELAST corresponding to the model MJ, but with zero imaginary parts of viscoelastic moduli; c) Model MJ ROT corresponding to the rotated model MJ; d) Model ORTHO, in which the real parts of viscoelastic moduli correspond to a perfectly elastic orthorhombic model of Schoenberg and Helbig [33], and imaginary parts are taken as in the model MJ; e) Model ORTHO ELAST, corresponding to the model of Schoenberg and Helbig .

Model MJ. We consider plane waves propagating in a medium of hexagonal symmetry whose complex-valued moduli were obtained by Jakobsen et al. [32]. We choose the model corresponding to the frequency of approximately 35 Hz and consider the density of 1000 kg/m^3. The 6×6 matrix $\boldsymbol{A}$ of complex-valued, density-normalized viscoelastic moduli of hexagonal symmetry with vertical axis of symmetry, measured in (km/s)^2, reads:

$$\boldsymbol{A} = \boldsymbol{A}_1 - i\boldsymbol{A}_2, \tag{9}$$

where

$$\boldsymbol{A}_1 = \begin{pmatrix} 46.631 & 5.983 & 4.278 & 0 & 0 & 0 \\ & 46.631 & 4.278 & 0 & 0 & 0 \\ & & 19.931 & 0 & 0 & 0 \\ & & & 13.444 & 0 & 0 \\ & & & & 13.444 & 0 \\ & & & & & 20.324 \end{pmatrix} \tag{10}$$

and

$$\boldsymbol{A}_2 = \begin{pmatrix} 0.033 & 0.022 & 0.156 & 0 & 0 & 0 \\ & 0.033 & 0.156 & 0 & 0 & 0 \\ & & 1.312 & 0 & 0 & 0 \\ & & & 0.055 & 0 & 0 \\ & & & & 0.055 & 0 \\ & & & & & 0.005 \end{pmatrix}. \tag{11}$$

Note that the matrices $\boldsymbol{A}_1$ and $\boldsymbol{A}_2$ are positively definite and the matrix $\boldsymbol{A}_1$ exhibits the kiss singularity along the vertical.

We study plane waves whose propagation-attenuation plane $\Sigma^{\|}$ coincides with a vertical symmetry plane Σ^S, and it is parallel to the plane (x, z). The components of the unit vectors **n** and **m** can thus be expressed as

$$n_1 = \sin i, n_2 = 0, n_3 = \cos i, m_1 = \cos i, m_2 = 0, m_3 = -\sin i, \quad (12)$$

where i is called the propagation angle.

For a better insight, we start with plots of the phase velocity of the *P* and *S* waves as functions of the propagation angle i in the symmetry plane Σ^S. We use the form of polar plots, in which $i = 0°$ upwards, $i = 90°$ to the right, see (12). In Fig. 1, phase velocity polar graphs for four values of the inhomogeneity parameter D, $D = 0$ (homogeneous wave), $D = 0.057$, $D = 0.059$, and $D = 0.2$, are shown. For $D = 0$, the phase velocities are symmetric with respect to the vertical axis. The phase-velocity surface corresponding to the fastest wave is separated from the remaining velocity surfaces and corresponds to the *P* wave. The higher of the remaining velocities corresponds to the *SH* wave (see particle motion diagrams in Fig. 2), the slower to the *SV* wave. Both *S*-wave phase velocities touch on the vertical axis. For increasing values of D, the *P*-wave and *SV*-wave phase velocity curves deform ($D = 0.057$) close to the vertical axis and approach each other. The *SV*-wave phase velocity curve intersects the *SH*-wave curve. The phase velocities are no more symmetric with respect to the vertical axis. With increasing D, the curves of the *P*- and *SV*-wave velocities get into contact, i.e., for the corresponding propagation angle i (which is nonzero), the *P* and *SV* waves propagate with the same phase velocity. With further increase of D, the phase velocities decrease (they become zero for $|D| \to \infty$) and all three phase-velocity curves become nearly indistinguishable. In viscoelastic or perfectly elastic *isotropic* media, the relevant curves of phase velocities of both *P* and *S* waves would be circular.

In the following plots of particle motion thickness of curves in the plots differs according to the phase velocity of the considered wave. The thickest curves correspond to the fastest, thinner to the intermediate and thin to the slowest wave. In the propagation-attenuation plane coinciding with Σ^S, the *SH* plane waves are polarized linearly, in the direction perpendicular to $\Sigma^{\|}$. The particle motion diagrams in the propagation-attenuation plane correspond to *P* and *SV* waves, the *SH* waves polarization being represented by points only.

Figure 2 shows particle motion diagrams for the inhomogeneity parameter $D = 0.02$. The polarization ellipses are plotted for twenty values of the propagation angle i, specifying the vector **n**, see (12). The vectors **n** point from the center of the figure toward the centers of polarization ellipses. We can see that both *P* and *SV* waves are elliptically polarized, with polarization ellipses mutually perpendicular. For some propagation angles, long axes of the polarization ellipses deviate considerably from the direction of **n** for *P* waves and from the direction perpendicular to **n** for *SV* waves. The deviations are minimum for horizontal and vertical directions, which represent longitudinal directions of the matrix $\boldsymbol{A}_1$. The eccentricity of the polarization ellipses varies significantly with the propagation angle. The eccentricities of the polarization ellipses of *P* and *S* waves for a given propagation angle are similar, but not the same. Particularly strong changes of eccentricity can be observed close to the vertical. In the perfectly elastic case, this is the direction of the kiss singularity. There is no symmetry in the orientation of the polarization ellipses and in their eccentricity with respect to the vertical. A full symmetry can be, however,

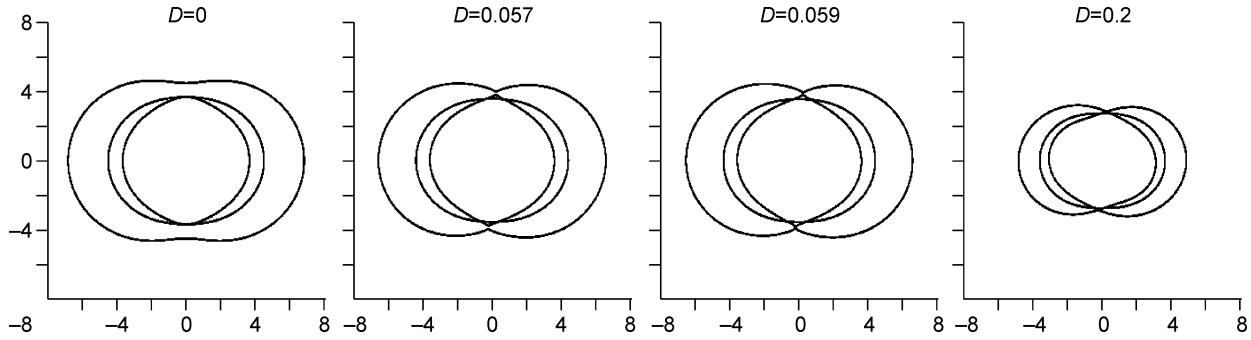

Fig. 1. Polar diagrams of the phase velocity C in a plane of symmetry of the model MJ for $D = 0$ (homogeneous wave), 0.057, 0.059 and 0.2. Outer curves: the fastest wave (*P* wave); the inner curves: *SV* and *SH* waves. *SV* wave is slowest except in directions close to the vertical for $D > 0$.

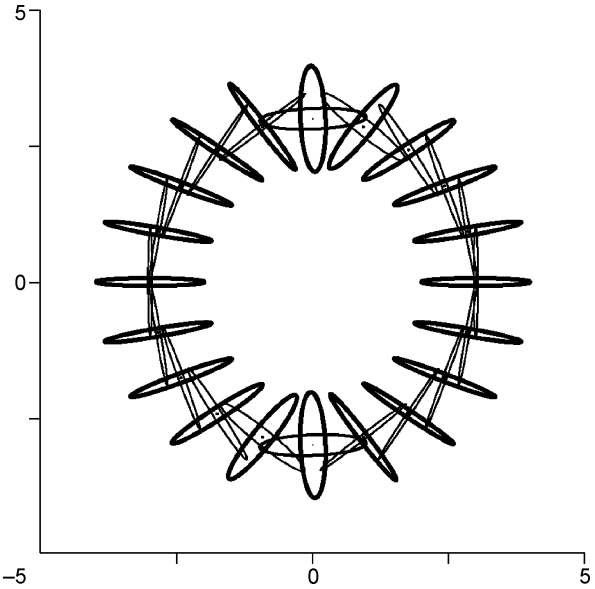

Fig. 2. Particle motion diagrams of *P* and *SV* waves in the same plane of the model MJ as in Fig. 1, for *D* = 0.02. Thickest curves: the fastest wave (*P* wave), thinner: intermediate wave, thin: the slowest wave. *SH* wave is polarized perpendicularly to the plane of symmetry.

observed for **n** and –**n**. Anomalous behavior of phase velocities of *SV* and *SH* waves can be observed. Note that along the vertical the *SV* wave becomes faster than the *SH* wave.

In Fig. 3, we investigate behavior of polarization for varying values of the inhomogeneity parameter *D*, namely for *D* = 0, 0.01, 0.02, 0.03, 0.05 and 0.1. The horizontal axis corresponds to the propagation angle *i*. The vertical direction corresponds to the direction of the vector **n**, perpendicular to the wavefront. In this presentation, the deviations of the longer axes of polarization ellipses of the *P* wave from the direction of **n** are particularly well pronounced. Note that for all *D*, the longer axis is parallel to **n** for *P* waves and perpendicular to it for *S* waves for $i = 90°$ only. For $i = 0°$, this is true only for a homogeneous plane wave, *D* = 0. With increasing *D*, the angle *i*, for which the two directions are parallel or perpendicular, shifts from zero to positive values. For $D = 0.1$ in Fig. 3, it is, approximately, $i = 5°$.

As we can see from Fig. 3, the polarization ellipses have very large eccentricity for homogeneous plane waves (*D* = 0). With increasing *D*, the eccentricity decreases. For *D* greater than those used in Fig. 3, *B*, the polarization ellipses become nearly circular. Consequently, for great *D*, it becomes difficult to distinguish *P* and *SV* waves according to their polarization. Also note that for increasing *D*, the range of propagation angles *i*, for which the *SV* wave propagates faster than the *SH* wave, also increases. All this also holds for negative values of *D*.

In Fig. 4, three important directions characterizing plane wave propagation in viscoelastic anisotropic media are compared. Particle motion diagrams as functions of the propagation angle, separately for *P*, *SV* and *SH* plane waves, are compared with corresponding directions of the time-averaged energy flux (short lines), and with vertical direction representing direction of the wavefront propagation. We can see that in regular regions (outside vicinity of the axis of symmetry, $i = 0°$), the direction of the energy flux is nearly parallel or perpendicular to the longer axes of the polarization ellipses. Both directions may deviate significantly from the direction of the wavefront propagation.

In the model MJ ELAST, the 6×6 matrix of density-normalized moduli is specified as $\boldsymbol{A} = \boldsymbol{A}_1$, see (9). Thus, we deal with a perfectly elastic anisotropic medium in this case. Let us compare the results for perfectly elastic anisotropic media with the results for viscoelastic anisotropic media, presented in previous section.

Figure 5 shows the same as Fig. 3, *A* but for a perfectly elastic anisotropic medium. For a homogeneous wave (*D* = 0), the polarization is strictly linear not only for *SH* wave but also for *P* and *SV* waves. For inhomogeneous plane waves ($D \neq 0$), the polarization of *P* and *SV* waves becomes elliptical.

Comparison of Figs. 3, *A* and 5 shows that the particle motion diagrams of *P* and *SV* waves in perfectly elastic and viscoelastic anisotropic media are very similar for a given *D* and *i*. This indicates that the perturbation

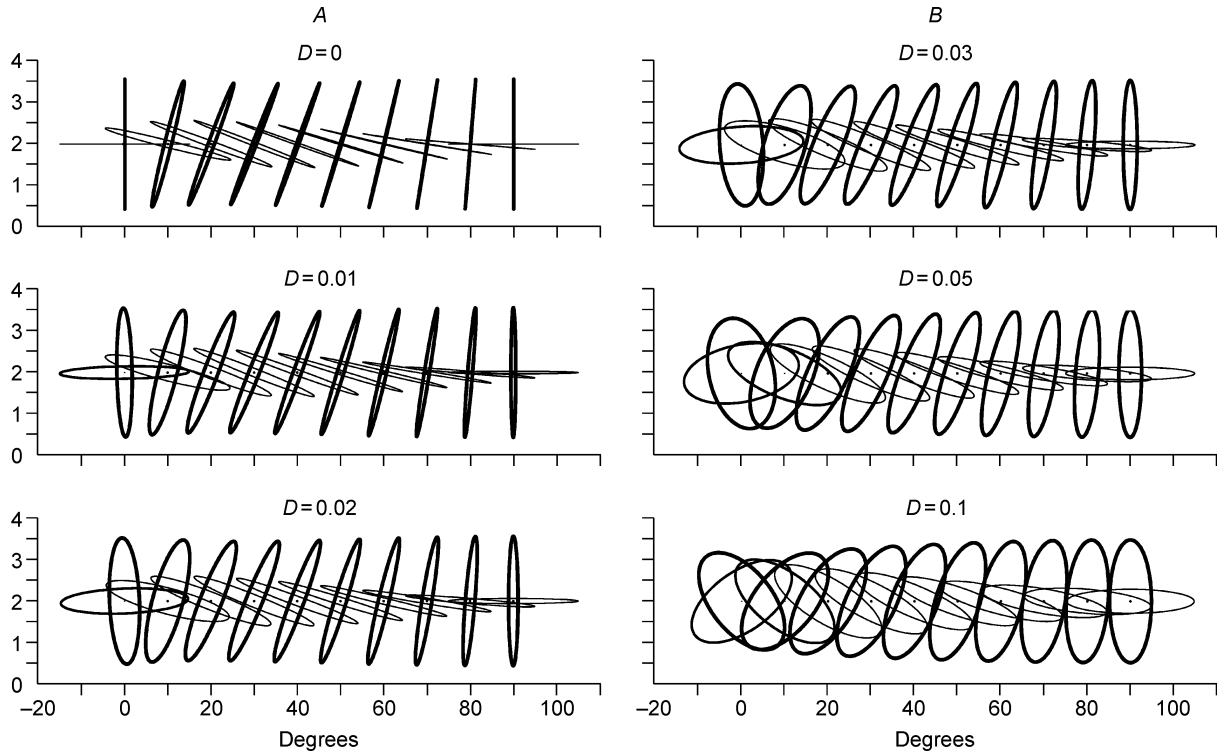

Fig. 3. Particle motion diagrams of *P* and *S* waves versus the propagation angle *i* in the same plane of the model MJ as in Fig. 2. *A* — for *D* = 0 (homogeneous wave), 0.01 and 0.02; *B* — for *D* = 0.03, 0.05 and 0.1. Direction of wavefront propagation is vertical. The use of different thicknesses as in Fig. 2. Thicker particle motion of the *SV* wave for *i* = 0° indicates that the *SV* wave is faster than *SH* wave in this direction.

methods for homogeneous as well as inhomogeneous plane waves propagating in weakly viscoelastic media, in which perfectly elastic media are used as a reference, should work very well.

Model MJ ROT. In this section, we wish to illustrate that the algorithm described in Section 1 works safely even outside symmetry planes. In such a case, we cannot speak about *SV* and *SH* waves any more, and thus we speak about S_1 (faster) and S_2 waves. We use the model MJ and rotate it by 40° about the x_2 axis, and then by 30° about the vertical (x_3 axis). Figure 6 shows projections of the particle motion diagrams into the propagation-attenuation plane $\Sigma^{\parallel}$. Because $\Sigma^{\parallel}$ does not coincide with the symmetry plane, we can observe particle motions of all three plane waves. The three plots in Fig. 6 correspond to D = 0, 0.01 and 0.02.

The particle motion diagrams in Fig. 6 have similar features as those in Figs. 3 and 5, specifically a decrease in the eccentricity with increasing D. Interesting is behavior of particle motions of the faster of the *S* waves in Fig. 6. It is polarized strictly horizontally for D = 0 and nearly horizontally for $D \neq 0$. The explanation of this phenomenon is simple. In a medium of hexagonal symmetry, every vector is situated in a plane of symmetry. Moreover, one of the *S* waves is polarized linearly and its particle motion is perpendicular to the plane of symmetry. Thus, a slowness vector of any homogeneous plane wave is situated in a plane of symmetry and is perpendicular to the polarization of the mentioned *S* wave. Since the slowness vectors in Fig. 6 are situated in the plane of the figure and are vertical, projection of the polarization of the considered *S* wave is horizontal. As D increases, the polarization of this wave also becomes elliptical and starts to deviate from the horizontal.

Model ORTHO. Let us now consider an orthorhombic model. The matrix $\boldsymbol{A}_1$, see (9), has been proposed by Schoenberg and Helbig [33]. It has the following form:

$$\boldsymbol{A}_1 = \begin{pmatrix} 9.00 & 3.60 & 2.25 & 0 & 0 & 0 \\ & 9.84 & 2.40 & 0 & 0 & 0 \\ & & 5.94 & 0 & 0 & 0 \\ & & & 2.00 & 0 & 0 \\ & & & & 1.60 & 0 \\ & & & & & 2.18 \end{pmatrix}. \qquad (13)$$

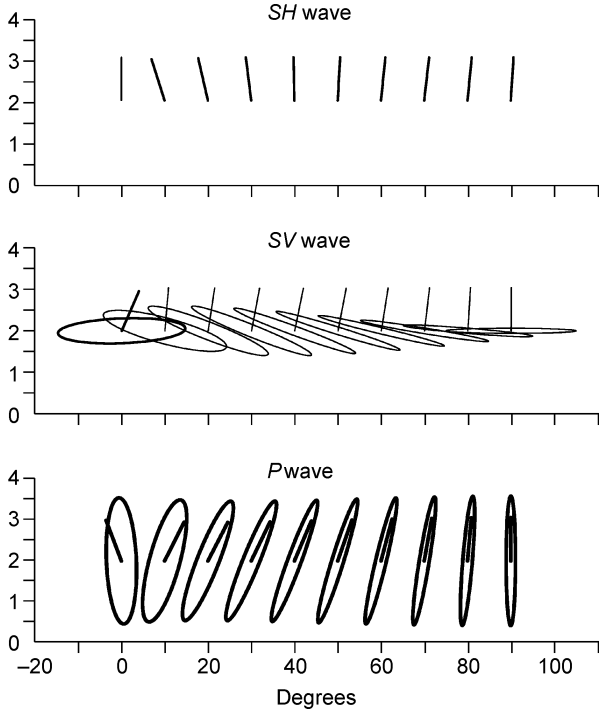

Fig. 4. Comparison of directions of the energy flux (short lines) and of the polarization ellipses for $D = 0.02$ for *P*, *SV* and *SH* waves in the model MJ. Direction of wavefront propagation is vertical.

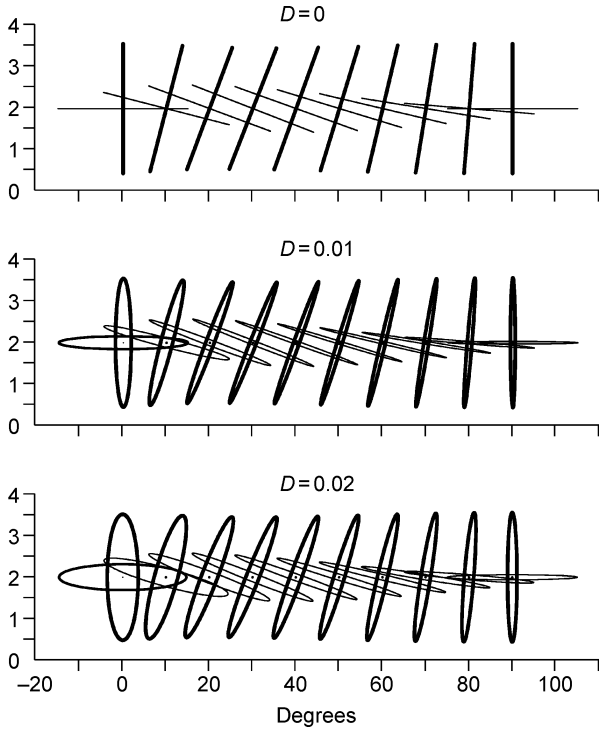

Fig. 5. The same as in Fig. 3, *A* but for the model MJ ELAST.

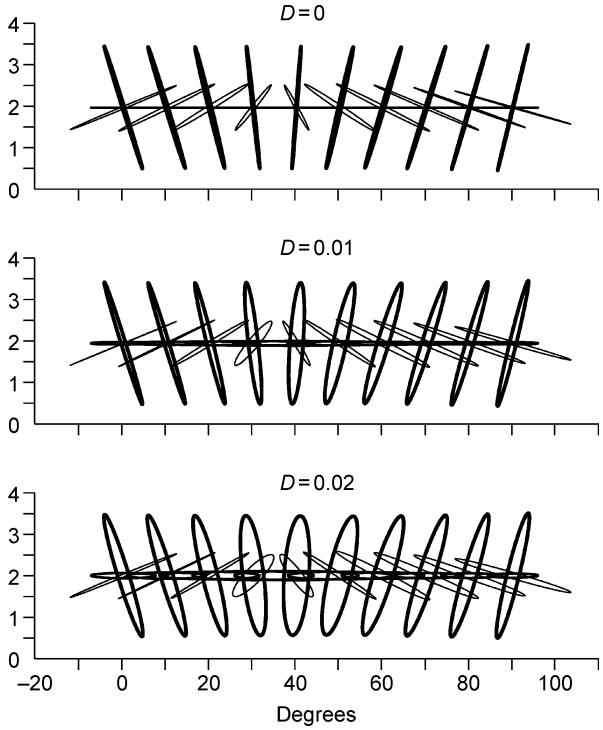

Fig. 6. The same as in Fig. 3 but for the model MJ ROT: rotated model of Fig. 2. Thick line — the *P* wave. Thin line — the slower *S* wave.

Voigt notation is again used, the elements of $\boldsymbol{A}_1$ are in $(\text{km/s})^2$. This model has two singularities (conical points) in the plane (x, z) for the propagation angles $i = 20.1°$ and 59.8°, one conical point in the plane (y, z) for the propagation angle $i = 72.5°$, and one more conical point for the propagation angle $i = 46.53°$ in the vertical plane deviating from (x, z) by 44.89°, [33].

In the model ORTHO, the matrix $\boldsymbol{A}_1$ is given by (13) and the matrix $\boldsymbol{A}_2$ is the same as in the model MJ, see (11).

In Figure 7, the particle motion diagrams are displayed in the propagation-attenuation plane $\Sigma^{\|}$ chosen so that it coincides with the plane of symmetry (x, z). The inhomogeneity parameter is $D = 0.02$. Figure 7 is analogous to Fig 2, with which it shares several common features. The differences are only in the propagation angles, for which the *SV* wave becomes faster than the *SH* wave. The *SV* wave is faster for the propagation angles approximately limited by conical points of the matrix $\boldsymbol{A}_1$, i.e., between ~20° and 60°. As in Fig. 2, the eccentricity of the polarization ellipses in Fig. 7 is minimum close to the directions, in which the *SV* wave is faster. It is interesting that the eccentricities of *P* and *SV* waves vary in a similar fashion.

In all the following plots, only particle motions of *S* waves are shown. Faster *S* wave is shown by thick curves, slower by thin ones. Variation of the particle motion with varying inhomogeneity parameter *D* in the same display as in Figs. 3–5 can be seen from Fig. 8. As in Fig. 7, we can see that with varying propagation angle one *S* wave becomes faster than the other, and vice versa. Except for some directions for $D = 0$, the polarization is elliptical. This is in contrast with the same plot of particle motion, but for the symmetry plane (y, z). As can be seen from Fig. 9, no matter how *D* varies, polarization of both waves is linear. While the polarization changes quite dramatically with the propagation angle, there is practically no variation with *D*. There is only one important exception. The propagation angle corresponding to the direction, in which both *S* waves propagate with the same phase velocity, decreases with increasing *D* as can be seen from the comparison of plots for $D = 0$ and $D = 0.04$ for $i \sim 70°$. Note significant deviations of the particle motion from the direction perpendicular to the direction of wavefront propagation.

Figure 10, A shows particle motion diagrams in the vertical plane deviating from (x, z) by 44.89°, i.e. in the plane, in which $\boldsymbol{A}_1$ has a conical singularity for the propagation angle 46.53°. We can see that eccentricity of polarization ellipses of one of the *S* waves (faster for the propagation angles less than 46.53°) is systematically

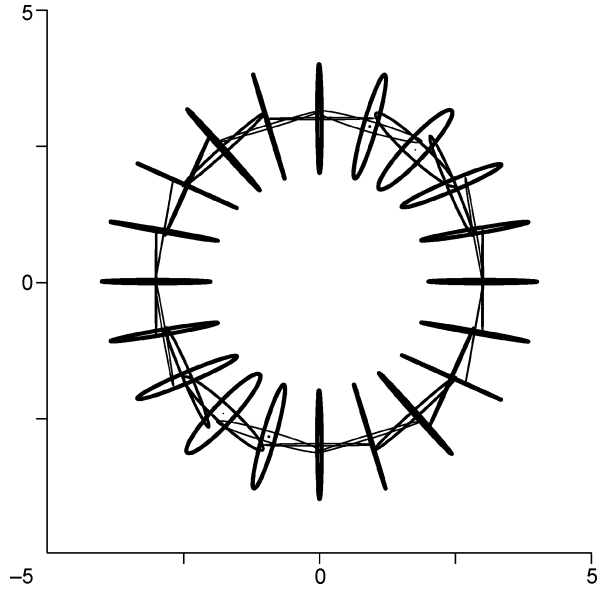

Fig. 7. Particle motion diagrams of *P* and *SV* waves for *D* = 0.02 in the (*x*, *z*) plane of symmetry of the model ORTHO. The use of different thicknesses as in Fig. 2. *SH* wave is polarized perpendicularly to the plane of symmetry. *SV* wave is faster for propagation angles *i* ~ 20–60°.

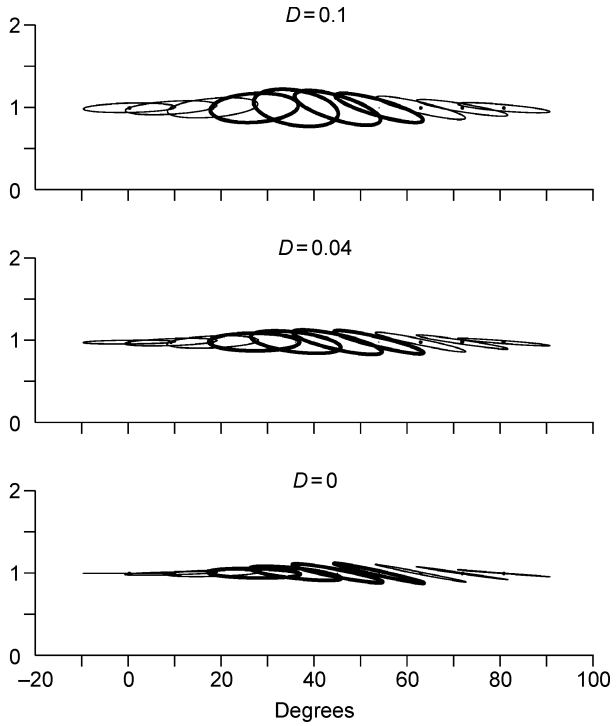

Fig. 8. Particle motion diagrams of *S* waves versus the propagation angle *i* for *D* = 0 (homogeneous wave), 0.04 and 0.1 in the (*x*, *z*) plane of the model ORTHO. Direction of wavefront propagation is vertical. Thicker curves are used for the particle motion of *S* wave with greater phase velocity. The *S* waves polarized as *SV* and *SH*. *SV* wave is faster for propagation angles *i* ~ 20–60°.

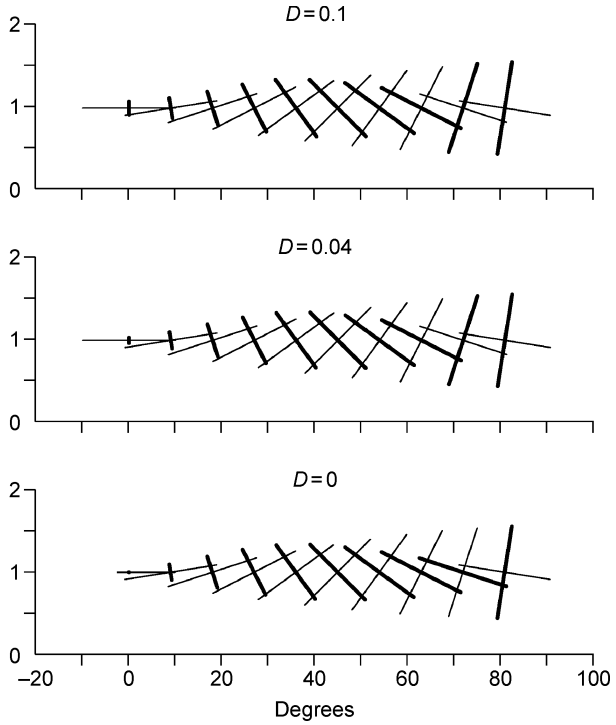

Fig. 9. Particle motion diagrams of *S* waves versus the propagation angle *i* for *D* = 0 (homogeneous wave), 0.04 and 0.1 in the (*y*, *z*) plane of the model ORTHO. Thicker curves used for the particle motion of *S* wave with greater phase velocity. Polarization of S_1 and S_2 waves changes abruptly between *i* = 70° and 80°. The angle of change varies with varying *D*. Note that both *S* waves are linearly polarized.

lower than of the other and that eccentricity decreases with decreasing propagation angles. Note again significant deviations of the particle motion from the direction perpendicular to the direction of wavefront propagation.

Model ORTHO ELAST. Here we consider the original model [33], i.e., $\boldsymbol{A}_1$ is given by (13) and the matrix $\boldsymbol{A}_2 = 0$. Except for $D = 0$, plots analogous to Fig. 9 are in this case very similar to those in Fig. 8. For $D = 0$, particle motion is strictly linear. Plots analogous to Fig. 10 are very similar to those in Fig. 9 even for $D = 0$. More pronounced differences can be seen in plots analogous to Fig. 10, *A*, see Fig. 10, *B*. For $D = 0$, particle motion is again strictly linear, for *D* nonzero, eccentricity of the polarization ellipses is very high.

CONCLUSIONS

The observations made on previous models can be summarized in the following way:

1. In most cases, both *P* and *SV* waves are elliptically polarized. Linear polarization can be observed along some specific directions, see, e.g., *SH* waves in symmetry planes of the MJ model or both *S* waves in the (*y*, *z*) symmetry plane of the model ORTHO. The longer axes of *P*- and *SV*-wave polarization ellipses are mutually perpendicular.

2. For some **n** the long axes of the polarization ellipses of *P* waves deviate considerably from the direction of **n**. The same holds for *SV* waves if the deviations are measured from the direction perpendicular to **n**.

3. The eccentricity of the polarization ellipses varies significantly with varying **n**.

4. The eccentricities of the polarization ellipses of *P* and *S* waves for a given **n** are similar but not the same.

5. There is no symmetry in the orientation of the polarization ellipses and in their eccentricity with respect to the vertical as in a perfectly elastic case. The symmetry exists for $D = 0$. With increasing $|D|$, asymmetry increases. A full symmetry can be observed for **n** and –**n**.

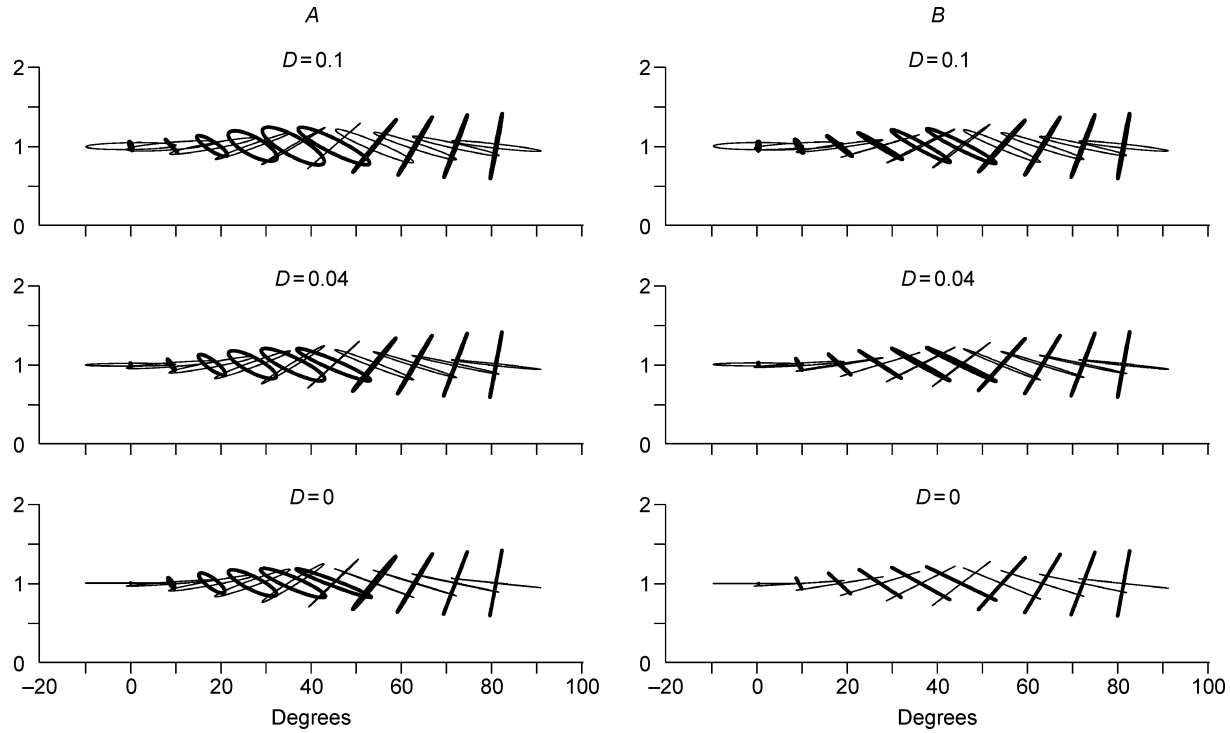

Fig. 10. Particle motion diagrams of *S* waves versus the propagation angle *i* for *D* = 0 (homogeneous wave), 0.04 and 0.1 in the vertical plane of the model ORTHO (*A*) making 44.89° with the (*x*, *z*) plane; the same for the model ORTHO ELAST (*B*). Thicker curves used for the particle motion of *S* wave with greater phase velocity. Polarization of S_1 and S_2 waves changes abruptly between *i* = 45° and 54°.

6. The direction of energy flux is usually closer to longer (shorter) axes of the polarization ellipses of *P* (*S*) waves than to the direction of **n**.

Acknowledgements. The authors greatly appreciate Sergei Goldin's important contribution to the theory of seismic wave propagation. Morten Jakobsen provided data for numerical examples. The research has been supported by the Consortium Project "Seismic Waves in Complex 3-D Structures", by the Research Projects 205/04/1104 and 205/05/2182 of the Grant Agency of the Czech Republic, and by the Research Project A3012309 of the Grant Agency of the Academy of Sciences of the Czech Republic.

REFERENCES

1. Aki, K., and P.G. Richards, *Quantitative seismology*, Freeman, San Francisco, 1980.

2. Kravtsov, Yu.A., and Yu.I. Orlov, *Geometrical optics of inhomogeneous media* [in Russian], Nauka, Moscow, 1980.

3. Petrashen', G.I., *Wave propagation in anisotropic elastic media* [in Russian], Nauka, Leningrad, 1980.

4. Fedorov, F.I., *Theory of elastic waves in crystals* [in Russian], 386 pp., Nauka, Moscow, 1965.

5. Helbig, K., *Foundations of anisotropy for exploration seismics*, Pergamon, Oxford, 1994.

6. Musgrave, M.J.P., *Crystal acoustics*, Holden Day, San Francisco 1970.

7. Borcherdt, R.D., Energy and plane waves in linear viscoelastic media, *J. Geophys. Res.*, **78**, 2442–2533, 1973.

8. Buchen, P.W., Plane waves in linear viscoelastic media, *Geophys. J. Roy. Astron. Soc.*, **23**, 531–542, 1971.

9. Carcione, J.M., *Wave fields in real media: Wave propagation in anisotropic, anelastic and porous media*, 316 pp., Pergamon, Amsterdam, 2001.

10. Caviglia, G., and A. Morro, *Inhomogeneous waves in solids and fluids*, 1–15, World Scientific, Singapore, 1992.

11. Krebes, E.S., Discrepancies in energy calculations for inhomogeneous waves, *Geophys. J. Roy. Astron. Soc.*, **75**, 839–846, 1983.

12. Carcione, J.M., and F. Cavallini, Energy balance and fundamental relations in anisotropic-viscoelastic media, *Wave Motion*, **18**, 11–20, 1993.

13. Carcione, J.M., and F. Cavallini, Forbidden directions for inhomogeneous pure shear waves in dissipative anisotropic media, *Geophysics*, **60**, 522–530, 1995.

14. Krebes, E.S., and L.H.T. Le, Inhomogeneous plane waves and cylindrical waves in anisotropic anelastic media, *J. Geophys. Res.*, **99**, B12, 23899–23919, 1994.

15. Romeo, M., Inhomogeneous waves in anisotropic dissipative solids, *Q.J. Mech. Appl. Math.*, **47**, 481–491, 1994.

16. Daley, P.F., and F. Hron, Reflection and transmission coefficients for transversely isotropic media, *Bull. Seismol. Soc. Amer.*, **67**, 661–676, 1977.

17. Gajewski, D., and I. Pšenčík, Computation of high-frequency seismic wavefileds in 3-D laterally inhomogeneous anisotropic media, *Geophys. J. Roy. Astron. Soc.*, **91**, 383–411, 1987.

18. Frazer, L.N., and G.J. Fryer, Useful properties of the system matrix for a homogeneous anisotropic visco-elastic solid, *Geophys. J.*, **97**, 173–177, 1989.

19. Kennett, B.L.N., *Seismic wave propagation in stratified media*, Cambridge Univ. Press, Cambridge, 1983.

20. Kennett, B.L.N., *The seismic wavefield. Vol. 1. Introduction and theoretical development*, Cambridge Univ. Press, Cambridge, 2001.

21. Thomson, C.J., *Notes on Rmatrix, a program to find the seismic plane-wave response of a stack of anisotropic layers*, Queen's University, Dept. of Geol. Sci., Kingston, 1996.

22. Thomson, C.J., *Notes on waves in layered media to accompany program Rmatrix*, Queen's University, Dept. of Geol. Sci., Kingston, 1996.

23. Woodhouse, J.H., Surface waves in laterally varying structure, *Geophys. J. Roy. Astron. Soc.*, **37**, 461–490, 1974.

24. Stroh, A.N., Steady state problems in anisotropic elasticity, *J. Math. Phys.*, **41**, 77–103, 1962.

25. Shuvalov, A.L., On the theory of plane inhomogeneous waves in anisotropic elastic media, *Wave Motion*, **34**, 401–429, 2001.

26. Shuvalov, A.L., and N.H. Scott, On the properties of homogeneous viscoelastic waves, *Q.J. Mech. Appl. Math.*, **52**, 405–417, 1999.

27. Shuvalov, A.L., and N.H. Scott, On singular features of acoustic wave propagation in weakly dissipative anisotropic thermoviscoelasticity, *Acta Mechanica*, **140**, 1–15, 2000.

28. Caviglia, G., and A. Morro, Existence and uniqueness in the reflection-transmission problem, *Q. J. Mech. Appl. Math.*, **52**, 543–564, 1999.

29. Červený, V., Inhomogeneous harmonic plane waves in viscoelastic anisotropic media, *Stud. Geophys. Geod.*, **48**, 167–186, 2004.

30. Červený, V., and I. Pšenčík, Plane waves in viscoelastic anisotropic media. Part 1: Theory, *Geophys. J. Int.*, **161**, 197–212, 2005.

31. Červený, V., and I. Pšenčík, Plane waves in viscoelastic anisotropic media. Part 2: Numerical examples, *Geophys. J. Int.*, **161**, 213–229, 2005.

32. Jakobsen, M., T.A. Johansen, and C. McCann, The acoustic signature of fluid flow in complex porous media, *J. Appl. Geophys.*, **54**, 219–246, 2003.

33. Schoenberg, M., and K. Helbig, Orthorhombic media: Modeling elastic wave behavior in a vertically fractured earth, *Geophysics*, **62**, 1954–1974, 1997.

Received 28 September 2005